

## Supporting Information

# Linear free energy relationships for transition metal chemistry: Case study of CH activation with copper-oxygen complexes

Zhenzhuo Lan,<sup>a</sup> and Shaama Mallikarjun Sharada<sup>\*a,b</sup>

## 1 Methods

**Simulation methods:** We use the ab initio quantum chemistry package, Q-Chem 5.1.2,<sup>1</sup> to carry out all density functional theory (DFT) simulations. Geometry optimization, transition state search,<sup>2,3</sup> and vibrational analysis of spin singlet structures are carried out using the range-separated, dispersion-corrected hybrid  $\omega$ B97X-D<sup>4,5</sup> functional. We utilize the Stuttgart Relativistic Small Core (srsc) effective core potential for Cu<sup>6</sup> and triple- $\zeta$  6-311+G\* basis set for the remaining atoms. Wavefunction stability analysis is used to determine broken-symmetry (BS) solutions.<sup>7,8</sup> The second-generation absolutely-localized molecular orbital (ALMO) flavor of energy decomposition analysis (EDA)<sup>9–14</sup> is utilized to calculate catalyst-substrate interaction energy differences ( $\Delta E_{INT}$ ) between transition states and initial states. The interaction energy ( $E_{INT}$ ) is given by

$$E_{INT} = E_{PRP} + E_{FRZ} + E_{POL} + E_{CT} \quad (1)$$

$E_{PRP}$  is the energy penalty required to prepare the fragments. In other words, it is the energy associated with distorting each of the two isolated fragments to the geometry that they have in the complex. Since it contributes to less than 1 kJ/mol for any system,  $E_{PRP}$  is neglected. Frozen interactions ( $E_{FRZ}$ ), or the energy difference between unrelaxed wavefunctions in the interacting fragments and isolated fragments, is further decomposed into permanent electrostatics or Coulombic interactions ( $E_{ELEC}$ ) and Pauli repulsion ( $E_{PAULI}$ ) caused by reduction in volume occupied by electrons upon bringing fragments close together. Polarization corresponds to the energy lowering caused by relaxing the frozen orbitals of each fragment ( $E_{POL}$ ) in the presence of the other, and the charge transfer term ( $E_{CT}$ ) is obtained from further *interfragment* relaxation of the orbitals.

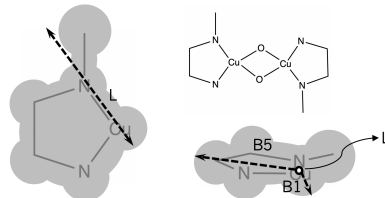


Figure 1: Illustration of Sterimol parameters for N-donor **13**. L is the total length along an axis defined by the Cu-N coordination. B1 and B5 are minimum and maximum widths of the group when looking down the L axis.

**Sterimol parameters:** Figure 1 illustrates the distances characterized by L, B1, and B5. We define the Cu-N axis closest to the substrate ( $\text{CH}_4$ ) as the primary axis to calculate L. Sterimol parameters are determined with Bondi radii<sup>15</sup> using the Python package developed by Brethomé A. V. *et al.*<sup>16</sup>

## 2 Validation: Catalyst geometries and CH activation barriers

We compare our structures for **23**, **26**, and **28** with EXAFS and DFT characterization studies carried out by Citek et al.<sup>17</sup> DFT-derived Cu-Cu, Cu-O and Cu-N bond lengths are in good agreement with each other and typically shorter than corresponding EXAFS values. Citek et al. also probe activation kinetics of CH bonds weaker (bond dissociation energy = 309.6 kJ/mol) than that of  $\text{CH}_4$ . We contrast these reaction rates with calculated barriers to verify whether trends are consistent. Table 1 depicts comparison of both bond lengths and kinetics. Decreasing rates from **23-28** is consistent with increase in our calculated barriers ( $\Delta E^\ddagger$ ), therefore serving to indirectly validate our methods and proposed mechanism.

<sup>a</sup> Mork Family Department of Chemical Engineering and Materials Science,

Table 1: Bond lengths ( $\text{\AA}$ ) for dicopper complexes with N-donors **23**, **26** and **28**. <sup>a</sup>Optimized at M06/TZVP/SMD(THF) level of theory. <sup>b</sup>This work. For complexes containing **26**, the catalyst geometry is not symmetric but more ‘*trans*’-like, leading to two distinct bond lengths. Experimental rate coefficients,  $k$ , are reported in  $\text{M}^{-1}\text{s}^{-1}$  and calculated barriers ( $\Delta E^\ddagger$ ) are in kJ/mol.

Source	Citek <i>et al.</i> , 2015 <sup>17</sup>				Current work				
	EXAFS (DFT <sup>a</sup> )			$k$	DFT <sup>b</sup>			$\Delta E^\ddagger$	
	Cu-Cu	Cu-O	Cu-N		Cu-Cu	Cu-O	Cu-N		
23		2.77(2.71)	1.86(1.80)	2.00(1.94)	9.2	2.73	1.79	1.94	101.3
26		2.82(2.75)	1.85(1.81)	2.01(1.98, 1.94)	0.4	2.75	1.79, 1.80	1.98, 1.94	123.5
28		2.85(2.83)	1.84(1.81)	2.02(2.00)	No Rxn	2.81	1.80	2.00	150.4

### 3 Oxo-insertion mechanism: Singlet state

Figure 2 depicts the potential energy surface for the singlet oxo-insertion mechanism proposed in our previous work.<sup>18</sup> The mechanism is concerted, and proceeds via simultaneous C–H and Cu–O bond breaking and C–O and O–H bond formation.

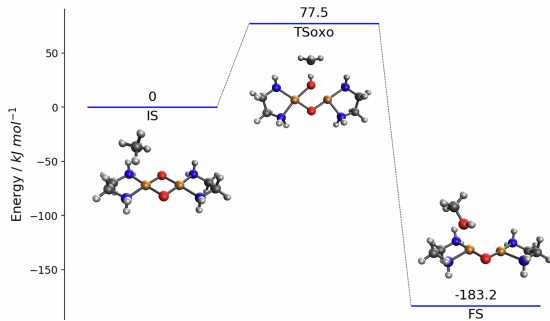


Figure 2: Potential energy diagram for the oxo-insertion mechanism of CH activation with **12**. X-axis represents reaction progress. **IS**, **TSoxo**, and **FS** correspond to initial, transition, and final states, respectively. Y-axis is the broken symmetry electronic energy (Cu: ochre, O: red, N: blue, C: grey).

### 4 Energy decomposition analysis

Table 2 reports  $\Delta E$ ’s or differences in EDA interaction energies and their constituents, strain energies, and barriers for the 33 systems under investigation. Figure 3 depicts  $\Delta\Delta E$ ’s, or EDA components and total interaction energy differences calculated using **1** as reference. For **1–25** and **29–33**, frozen interactions span a wide range, becoming more repulsive with increasing steric bulk. However, they are almost exactly cancelled by changes in polarization energies arising from the fact that larger N-donors are also more polarizable. **26–28** deviate from these trends largely on account of more repulsive catalyst-substrate charge transfer interactions arising from N-donor deformations in the direction opposite to the substrate in the transition state.

### 5 Catalyst strain in **26–28**

Apart from Cu–O stretch, catalysts **1–25** and **29–33** exhibit very small deformations (strain) in the transition state. On the other hand, large out-of-plane bending is observed for **26–28**. This bending can be described in terms of the change in torsion angle,  $\Delta\text{N}-\text{O}-\text{O}-\text{N}$ . The out-of-plane bending for **28** is illustrated in Table 3.

<sup>b</sup> Department of Chemistry, University of Southern California, Los Angeles CA 90089, USA.  
E-mail: ssharada@usc.edu

Table 2: EDA components (kJ/mol) for oxo-insertion with N-donors **1-33** – frozen ( $\Delta E_{FRZ}$ ), polarization ( $\Delta E_{POL}$ ), charge transfer ( $\Delta E_{CT}$ ), total interaction ( $\Delta E_{INT}$ ), electrostatic ( $\Delta E_{ELEC}$ ) and Pauli repulsion energies ( $\Delta E_{PAULI}$ ).

N-donor	$\Delta E_{FRZ}$	$\Delta E_{POL}$	$\Delta E_{CT}$	$\Delta E_{INT}$	$\Delta E_{ELEC}$	$\Delta E_{PAULI}$
1	561.6	-76.0	-537.4	-51.8	-306.4	868.0
2	585.4	-89.2	-545.8	-49.6	-325.4	910.8
3	602.6	-101.6	-544.4	-43.3	-342.4	945.0
4	597.0	-100.1	-540.3	-43.4	-338.8	935.8
5	623.4	-119.1	-548.1	-43.8	-360.7	984.1
6	646.8	-138.0	-550.5	-41.7	-381.4	1028.2
7	576.5	-83.9	-538.3	-45.7	-320.0	896.4
8	580.0	-85.8	-537.8	-43.7	-322.8	902.8
9	580.8	-86.4	-537.1	-42.6	-323.6	904.4
10	582.6	-87.8	-537.0	-42.3	-326.9	909.5
11	585.1	-88.7	-538.7	-42.3	-327.0	912.1
12	599.0	-100.8	-550.2	-52.0	-345.5	944.5
13	617.6	-118.1	-549.7	-50.2	-368.5	986.1
14	629.5	-125.5	-547.5	-43.5	-374.8	1004.3
15	634.0	-129.2	-549.8	-45.0	-378.5	1012.5
16	648.7	-149.4	-545.2	-45.9	-397.2	1045.9
17	656.1	-153.4	-543.9	-41.2	-397.5	1053.6
18	604.2	-108.8	-548.3	-52.9	-354.9	959.1
19	613.5	-111.3	-549.8	-47.6	-358.4	971.9
20	611.0	-109.0	-546.0	-44.0	-355.1	966.1
21	610.9	-109.7	-545.3	-44.1	-355.5	966.4
22	615.4	-112.2	-549.4	-46.2	-359.1	974.5
23	618.8	-118.1	-549.4	-48.8	-367.5	986.3
24	629.7	-131.2	-544.3	-45.7	-378.7	1008.5
25	662.0	-156.0	-547.6	-41.6	-412.5	1074.5
26	622.5	-119.7	-534.7	-31.8	-365.8	988.4
27	616.6	-118.5	-525.5	-27.4	-354.8	971.5
28	619.0	-120.4	-520.3	-21.7	-359.5	978.5
29	621.7	-120.4	-545.3	-44.1	-370.5	992.2
30	616.0	-114.9	-540.3	-39.1	-364.3	980.3
31	622.3	-121.0	-542.0	-40.7	-370.7	993.1
32	626.5	-124.4	-544.7	-42.6	-374.2	1000.7
33	627.0	-125.7	-544.5	-43.2	-374.8	1001.8

## 6 Determination of steric descriptors

A linear combination of  $B1$  and  $\theta$  differences between the chosen and reference systems constitutes a reliable descriptor for strain energies. We consider other combinations of descriptors, including  $(\Delta L, \Delta \theta)$  and  $(\Delta B1, \Delta L)$ . However, as seen below in Figure 4 and 5, the linear fits are poorer (lower  $R^2$ ) compared to the model obtained using  $(\Delta B1, \Delta \theta)$ . If we choose  $(\Delta L, \Delta \theta)$ , the parameters fail to capture substitutions at N-atoms. On the other hand,  $(\Delta B1, \Delta L)$  do not adequately describe changes to the N-donor backbone.

## 7 Transferability tests

**Asymmetric substitutions:** We determine the validity of the Taft-like correlation for strain effects by asymmetrically associating the  $[Cu_2O_2]^{2+}$  center with N-donors chosen from **1-25** and **29-33** to create 30 model catalysts. In the model calculations, we approximate the bite angles as those determined for the original **1-25**, **29-33** systems. This is a reasonable assumption since the bite angles deviate, on average, by < 0.5%. Similar assumptions are made for  $B1$ . Table 4 reports both calculated results, predicted strain energies and model errors.

**Level of theory:** To test model transferability, we carry out simulations and recalculate Sterimol parameters and bite angles at the SCAN,<sup>19</sup> B3LYP<sup>20</sup> and  $\omega$ B97M-V<sup>21</sup> level of theory with the same basis set. Table 5 reports calculated results and model predictions with the reference set to **1** at the new level of theory.

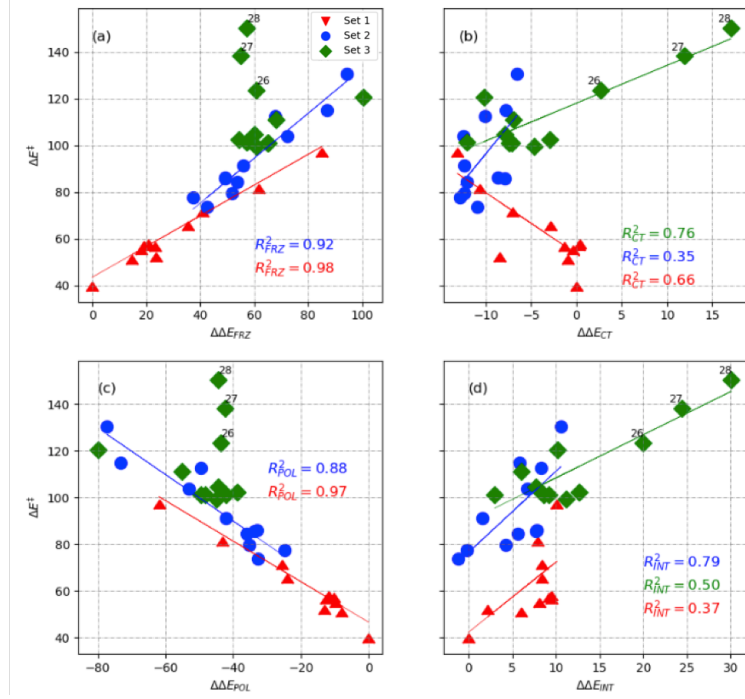


Figure 3:  $\Delta\Delta E_{INT}$  and its components for oxo-insertion barriers: (a) frozen, (b) charge transfer, (c) polarization, and (d) total interaction energies. Data labels correspond to the indices of N-donors. All results are reported with **1** as the reference state. Solid lines correspond to linear fits and corresponding  $R^2$  values are reported in the plot.

Table 3: Lateral views of **IS** with a planar active site and N-atoms and **TSoxo** with an out-of-plane N-atom for **28**.

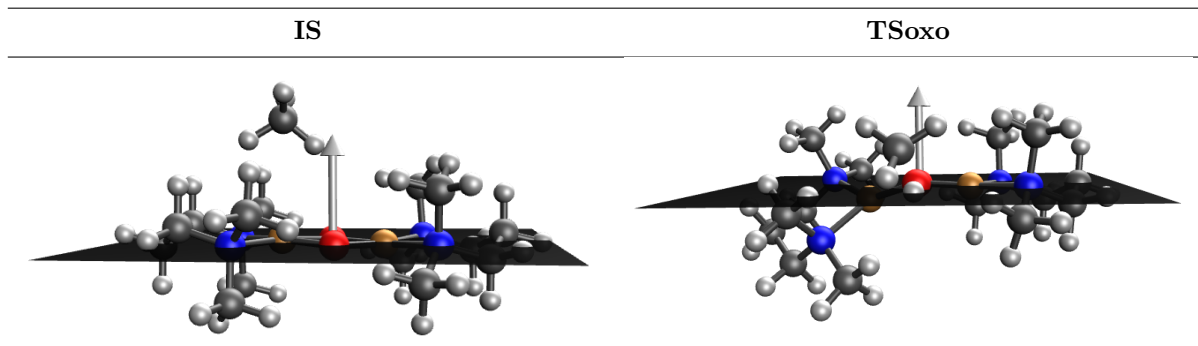


Table 4: Calculated  $\Delta E^\ddagger$ ,  $\Delta E_{INT}$ , and  $\Delta E_{STR}$  for 30 catalysts with asymmetrically substituted  $[\text{Cu}_2\text{O}_2]^{2+}$ .  $\Delta E_{STR,model}$  corresponds to model predictions based on Equation 4 in the main text. All energies are in kJ/mol. Mean error is 0.3kJ/mol standard deviation is 4.4kJ/mol.

N-donor 1	N-donor 2	$\Delta B1_1 + \Delta B1_2$ (Å)	$\Delta E^\ddagger$	$\Delta E_{INT}$	$\Delta E_{STR}$	$\Delta E_{STR,model}$	Error
1	2	0.00	43.3	-50.1	93.4	93.7	0.3
1	3	0.36	53.0	-45.4	98.3	100.5	2.2
1	4	0.00	47.7	-47.9	95.6	93.9	-1.7
1	5	1.22	77.9	-46.3	124.2	116.1	-8.1
1	6	1.22	62.9	-49.2	112.2	116.8	4.6
2	3	0.74	61.8	-44.0	105.8	107.7	2.0
2	4	0.36	57.8	-43.8	101.6	100.7	-0.9
2	5	0.75	67.2	-44.3	111.5	108.2	-3.3
2	6	1.61	72.5	-44.0	116.5	124.2	7.7
3	4	0.36	70.9	-42.4	113.3	101.2	-12.1
3	5	0.75	75.7	-37.4	113.1	108.6	-4.5
3	6	1.58	82.0	-39.1	121.0	124.1	3.1
4	5	1.22	77.0	-40.8	117.8	116.8	-1.1
4	6	1.22	77.1	-42.7	119.8	117.5	-2.3
5	6	1.61	88.3	-39.9	128.2	124.9	-3.3
1	12	0.05	56.0	-49.5	105.5	110.4	4.9
1	13	0.08	59.5	-49.9	109.4	111.7	2.3
1	14	0.41	74.8	-41.7	116.5	118.1	1.6
1	23	0.08	65.6	-48.4	114.0	120.4	6.4
1	24	0.11	75.3	-41.6	116.8	119.9	3.1
1	25	0.45	81.3	-41.6	122.9	126.1	3.2
12	23	0.13	91.7	-47.4	139.1	137.5	-1.5
12	24	0.16	98.2	-43.9	142.1	137.1	-5.1
12	25	0.50	97.8	-42.3	140.1	143.3	3.2
17	23	1.35	115.9	-44.7	160.5	161.8	1.2
17	24	1.38	113.1	-40.1	153.1	161.3	8.2
17	25	1.72	127.0	-40.0	167.0	167.5	0.5
23	24	0.19	105.4	-41.6	146.9	147.1	0.1
23	25	0.53	116.7	-37.6	154.3	153.3	-1.0
24	25	0.56	118.4	-35.2	153.5	152.8	-0.7

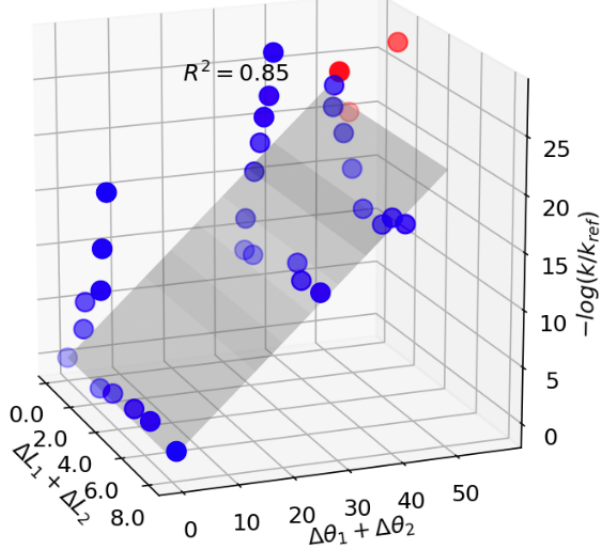


Figure 4: Correlation of strain energies with the combination of bite angle ( $^{\circ}$ ) and Sterimol L ( $\text{\AA}$ ),  $-\log(k/k_{ref}) = -0.01(\Delta L_1 + \Delta L_2) + 0.44(\Delta\theta_1 + \Delta\theta_2)$ , with  $R^2 = 0.85$ .

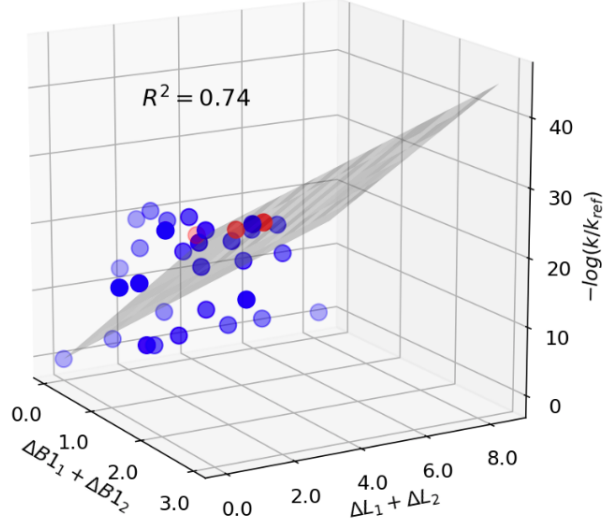


Figure 5: Correlation of strain energies with with the combination of Sterimol B1 and L parameters ( $\text{\AA}$ ),  $-\log(k/k_{ref}) = 9.93(\Delta B1_1 + \Delta B1_2) + 1.73(\Delta L_1 + \Delta L_2)$ , with  $R^2 = 0.74$ .

Table 5:  $\Delta E^{\ddagger}$ ,  $\Delta E_{INT}$ , and  $\Delta E_{STR}$  (kJ/mol) for **1**, **12**, and **23** calculated in SCAN, B3LYP, and  $\omega$ B97M-V level of theory. Results of the model are labeled  $\Delta E_{STR,model}$ .

Functional	N-donor	Bite angle	Sterimol Parameters ( $\text{\AA}$ )			$\Delta E^{\ddagger}$	$\Delta E_{INT}$	$\Delta E_{STR}$	$\Delta E_{STR,model}$	Error
			$\theta$ ( $^{\circ}$ )	$L_1, L_2$	$B1_1, B1_2$					
meta-GGA	1	73.392	4.13	1.55	3.62, 3.61	71.1	-170.3	241.5	241.5	0.0
	SCAN	87.263	4.95, 4.94	1.61	4.47	97.6	-174.2	271.8	273.5	1.7
global hybrid	23	95.662	5.16, 5.15	1.64, 1.63	4.91, 4.92	114.0	-171.0	285.0	292.5	7.5
	B3LYP	71.416	4.17, 4.21	1.55	3.64, 3.67	31.7	-156.6	188.3	188.3	0.0
meta-GGA hybrid	12	86.517	4.98, 5.02	1.61	4.48, 4.51	68.9	-156.7	225.6	222.9	-2.7
	23	95.417	5.21, 5.25	1.64	4.95, 4.99	89.1	-156.7	245.8	243.1	-2.7
$\omega$ B97M-V	1	72.280	4.17, 4.14	1.55	3.64, 3.63	51.9	-21.3	73.2	73.2	0.0
	12	87.338	4.98, 4.95	1.61, 1.60	4.48, 4.47	92.2	-22.2	114.4	107.6	-6.8
	23	95.989	5.21, 5.16	1.64, 1.63	4.95, 4.92	116.8	-15.0	131.7	127.3	-4.4

## References

- [1] Y. Shao, Z. Gan, E. Epifanovsky, A. T. Gilbert, M. Wormit, J. Kussmann, A. W. Lange, A. Behn, J. Deng, X. Feng, D. Ghosh, M. Goldey, P. R. Horn, L. D. Jacobson, I. Kaliman, R. Z. Khalilullin, T. Kuš, A. Landau, J. Liu, E. I. Proynov, Y. M. Rhee, R. M. Richard, M. A. Rohrdanz, R. P. Steele, E. J. Sundstrom, H. L. W. III, P. M. Zimmerman, D. Zuev, B. Albrecht, E. Alguire, B. Austin, G. J. O. Beran, Y. A. Bernard, E. Berquist, K. Brandhorst, K. B. Bravaya, S. T. Brown, D. Casanova, C.-M. Chang, Y. Chen, S. H. Chien, K. D. Closser, D. L. Crittenden, M. Diedenhofen, R. A. D. Jr., H. Do, A. D. Dutoi, R. G. Edgar, S. Fatehi, L. Fusti-Molnar, A. Ghysels, A. Golubeva-Zadorozhnaya, J. Gomes, M. W. Hanson-Heine, P. H. Harbach, A. W. Hauser, E. G. Hohenstein, Z. C. Holden, T.-C. Jagau, H. Ji, B. Kaduk, K. Khistyaev, J. Kim, J. Kim, R. A. King, P. Klunzinger, D. Kosenkov, T. Kowalczyk, C. M. Krauter, K. U. Lao, A. D. Laurent, K. V. Lawler, S. V. Levchenko, C. Y. Lin, F. Liu, E. Livshits, R. C. Lochan, A. Luenser, P. Manohar, S. F. Manzer, S.-P. Mao, N. Mardirossian, A. V. Marenich, S. A. Maurer, N. J. Mayhall, E. Neuscamman, C. M. Oana, R. Olivares-Amaya, D. P. O'Neill, J. A. Parkhill, T. M. Perrine, R. Peverati, A. Prociuk, D. R. Rehn, E. Rosta, N. J. Russ, S. M. Sharada, S. Sharma, D. W. Small, A. Sodt, T. Stein, D. Stück, Y.-C. Su, A. J. Thom, T. Tsuchimochi, V. Vanovschi, L. Vogt, O. Vydriv, T. Wang, M. A. Watson, J. Wenzel, A. White, C. F. Williams, J. Yang, S. Yeganeh, S. R. Yost, Z.-Q. You, I. Y. Zhang, X. Zhang, Y. Zhao, B. R. Brooks, G. K. Chan, D. M. Chipman, C. J. Cramer, W. A. G. III, M. S. Gordon, W. J. Hehre, A. Klamt, H. F. S. III, M. W. Schmidt, C. D. Sherrill, D. G. Truhlar, A. Warshel, X. Xu, A. Aspuru-Guzik, R. Baer, A. T. Bell, N. A. Besley, J.-D. Chai, A. Dreuw, B. D. Dunietz, T. R. Furlani, S. R. Gwaltney, C.-P. Hsu, Y. Jung, J. Kong, D. S. Lambrecht, W. Liang, C. Ochsenfeld, V. A. Rassolov, L. V. Slipchenko, J. E. Subotnik, T. V. Voorhis, J. M. Herbert, A. I. Krylov, P. M. Gill and M. Head-Gordon, *Molecular Physics*, 2015, **113**, 184–215.
- [2] A. Behn, P. M. Zimmerman, A. T. Bell and M. Head-Gordon, *The Journal of Chemical Physics*, 2011, **135**, 224108.
- [3] S. Mallikarjun Sharada, P. M. Zimmerman, A. T. Bell and M. Head-Gordon, *Journal of Chemical Theory and Computation*, 2012, **8**, 5166–5174.
- [4] J.-D. Chai and M. Head-Gordon, *Physical Chemistry Chemical Physics*, 2008, **10**, 6615–6620.
- [5] J.-D. Chai and M. Head-Gordon, *The Journal of Chemical Physics*, 2008, **128**, 084106.
- [6] M. Dolg, U. Wedig, H. Stoll and H. Preuss, *The Journal of Chemical Physics*, 1987, **86**, 866–872.
- [7] R. Bauernschmitt and R. Ahlrichs, *The Journal of Chemical Physics*, 1996, **104**, 9047–9052.
- [8] S. Mallikarjun Sharada, D. Stuck, E. J. Sundstrom, A. T. Bell and M. Head-Gordon, *Molecular Physics*, 2015, **113**, 1802–1808.
- [9] R. Z. Khalilullin, E. A. Cobar, R. C. Lochan, A. T. Bell and M. Head-Gordon, *The Journal of Physical Chemistry A*, 2007, **111**, 8753–8765.
- [10] P. R. Horn, E. J. Sundstrom, T. A. Baker and M. Head-Gordon, *The Journal of Chemical Physics*, 2013, **138**, 134119.
- [11] P. R. Horn and M. Head-Gordon, *The Journal of Chemical Physics*, 2015, **143**, 114111.
- [12] P. R. Horn and M. Head-Gordon, *The Journal of Chemical Physics*, 2016, **144**, 084118.
- [13] P. R. Horn, Y. Mao and M. Head-Gordon, *The Journal of Chemical Physics*, 2016, **144**, 114107.
- [14] P. R. Horn, Y. Mao and M. Head-Gordon, *Physical Chemistry Chemical Physics*, 2016, **18**, 23067–23079.
- [15] A. Bondi, *The Journal of Physical Chemistry*, 1964, **68**, 441–451.
- [16] A. V. Brethomé, S. P. Fletcher and R. S. Paton, *ACS Catalysis*, 2019, **9**, 2313–2323.
- [17] C. Citek, S. Herres-Pawlis and T. D. P. Stack, *Accounts of Chemical Research*, 2015, **48**, 2424–2433.
- [18] Z. Lan and S. Mallikarjun Sharada, *Physical Chemistry Chemical Physics*, 2018, **20**, 25602–25614.
- [19] J. Sun, A. Ruzsinszky and J. P. Perdew, *Physical Review Letters*, 2015, **115**, 036402.
- [20] A. D. Becke, *The Journal of Chemical Physics*, 1993, **98**, 5648–5652.
- [21] N. Mardirossian and M. Head-Gordon, *The Journal of Chemical Physics*, 2016, **144**, 214110.